A more accurate estimation of fracture weaknesses constrained using fracture facies

Huaizhen Chen[1,2], Jian Han[1], Kris Innanen[2]

ABSTRACT

Establishment of model constraints is crucial for seismic inversion. Well-logging data is usually used to generate initial models in the case of estimating elastic parameters (e.g. P- and S-wave velocities, impedances and moduli, etc.). However, in the case of seismic inversion for fracture indicators (e.g. weakly anisotropy parameters, fracture weaknesses), conventional well logging data cannot be directly used to build initial models of fracture indicators. To implement a better estimation of fracture weaknesses, we propose a two-stage inversion method, which is implemented as: 1) estimating azimuthal elastic impedance (AEI) and fracture facies; and 2) predicting fracture weaknesses using the estimated AEI as the input and model constraints constructed using the predicted fracture facies. In the first stage, we use Gaussian mixture prior distribution to obtain the AEI of different incidence angles and azimuths, and predict the fracture facies according to Bayesian classification; and in the second-stage, we implement a model-constrained Bayesian inversion for fracture weaknesses. We apply the proposed two-stage inversion method to synthetic seismic data, which illustrates the inversion method is robust even in the case of employing noisy seismic data of signal-to-noise ratio (S/N) of 1 as the input. Example of real data reveals that reliable results of fracture weaknesses are obtained using the proposed inversion method, which verifies that our method is a valuable tool for generating reliable fracture indicators from azimuthal seismic data.

INTRODUCTION

In hydrocarbon reservoirs, natural fractures are important channels for hydrocarbon accumulation and migration, and geophysicists place the effort on how to employ seismic data to estimate fracture indicators and improve the accuracy of inversion for fracture parameters (e.g. fracture density, fracture filling modulus).

To model how fracture parameters influence seismic wave propagation in fractured rocks, a cracked rock model proposed by Hudson (1980) and a fractured rock model given by Schoenberg and Douma (1988) are employed to involve the effect of fracture parameters in the rock stiffness matrix. In fractured rock model, two variables, i.e. the normal fracture weakness δ_{N} and the tangential fracture weakness δ_{T}, are presented and employed as the indicators of underground fractures because of δ_{N} and δ_{T} increasing with fracture density monotonously.

To predict underground fractured zones, Chen et al. (2015) formulated PP-wave reflection coefficient in terms of δ_{N} and δ_{T} and implement the inversion of azimuthal seismic data for estimating elastic parameters and fracture weaknesses simultaneously. To improve

1. Tongji University, Shanghai, China.
2. CREWES Project, University of Calgary, Canada.

the accuracy of fracture prediction and identify fracture filling fluid type, Chen et al. (2018) presented PP-wave reflection coefficient as a function of the modified fluid factor and dry fracture weaknesses, and implement the inversion of azimuthal seismic data for azimuthal elastic impedance (AEI) and the inversion of AEI for fluid factor and dry fracture weaknesses using Bayesian Markov chain Monte Carlo (MCMC) method. However, due to the existence of errors in observed seismic data and the crosstalk between the elastic parameters and fracture weaknesses and between fracture weaknesses themselves, it is difficult to obtain inversion results of fracture weaknesses of high accuracy without more reliable model constraints being involved in the inversion.

A reliable estimation of facies contributes to the characterization of reservoir lithology. Grana and Della Rossa (2010) proposed the method and workflow of seismic inversion for petrophysical-properties estimation based on statistical rock physics and implemented the lithology-fluid probabilistic classification for reservoir characterization. Grana et al. (2017) presented how to involve Gaussian mixture models in Bayesian inversion method and how to apply the method to seismic inversion and reservoir characterization. Grana (2018) developed a method of employing seismic data to simultaneously estimate facies and reservoir properties, in which the mixture distribution is also followed to formulate the objective function. Li et al. (2022) presented the multi-trace Markov chain Monte Carlo (MCMC) method of using data of seismic amplitude variation witho offset (AVO) to estimate reservoir parameters. Currently, the predicted lithology and fluid facies are preserved as valuable information for hydrocarbon reservoir characterization. However, the further application of predicted facies in seismic inversion remains to be studied.

Focusing on fractured reservoirs, we first present the fracture facies that is similar to lithology facies, which indicates the location where fractures exist. Following Grana (2018), we present a method of employing azimuthal partially incidence-angle-stacked seismic data to estimate azimuthal elastic impedance (AEI) and fracture facies at different incidence angles and azimuths. With the estimated fracture facies at different incidence and azimuths in hand, we select the unique and final fracture facies. The selected fracture facies is used to build initial models of fracture weaknesses, which reveals that the predicted fracture facies is further used in seismic inversion. Using the initial models constructed using fracture facies as the constraint and the estimated AEI as the input, we implement the Bayesian maximum a posterior (MAP) inversion for elastic properties and fracture weaknesses. Tests on synthetic seismic data illustrate that the proposed method that employs the predicted fracture facies to build the initial models of unknown parameters may provide more accurate inversion results of fracture weaknesses than that uses the traditional low-frequency initial model. Examples of real seismic data demonstrate the reliable fracture weaknesses are obtained using the proposed inversion method. We conclude that the proposed method is a valuable tool for producing indicators of fractured reservoirs.

THEORY AND METHOD

In this section, we propose the two-stage inversion method and present how to implement the inversion of azimuthal seismic data for estimating AEI and fracture facies, how to build initial models using the estimated fracture facies, and how to use the estimated AEI to predict fracture weaknesses.

Seismic inversion for AEI and fracture facies

For the interface separating two layers that contain a set of vertically aligned fractures, Chen et al. (2017) derive PP-wave reflection coefficient $R_{\rm PP}$ in terms of P- and S-wave velocities and fracture weaknesses. Following Chen et al. (2017), we express $R_{\rm PP}$ as a function of P- and S-wave moduli and fracture weaknesses

$$R_{\rm PP}(\theta,\phi) = a_M(\theta)\frac{\Delta M}{2M} + a_\mu(\theta)\frac{\Delta\mu}{2\mu} + a_\rho(\theta)\frac{\Delta\rho}{2\rho} + a_{\rm N}(\theta,\phi)\,\Delta\delta_{\rm N} + a_{\rm T}(\theta,\phi)\,\Delta\delta_{\rm T}, \tag{1}$$

where θ is the incidence angle, ϕ is the azimuthal angle, M, μ and ρ are P- and S-wave moduli and density, ΔM, $\Delta\mu$, $\Delta\rho$, $\Delta\delta_{\rm N}$ and $\Delta\delta_{\rm T}$ are changes in P- and S-wave moduli, density and fracture weaknesses of layers across the interface, and

$$\begin{aligned} a_M(\theta) &= \frac{\sec^2\theta}{2} \\ a_\mu(\theta) &= -4\,g\sin^2\theta \\ a_\rho(\theta) &= \frac{\cos 2\theta}{2\cos^2\theta} \\ a_{\rm N}(\theta,\phi) &= -\frac{1}{4\cos^2\theta}\left[2\,g\left(\cos^2\theta + \sin^2\theta\sin^2\phi\right) - 1\right]^2 \\ a_{\rm T}(\theta,\phi) &= g\sin^2\theta\cos^2\phi\left(\tan^2\theta\sin^2\phi - 1\right) \end{aligned} \tag{2}$$

where $g = \mu/M$.

Following Chen et al. (2018), we derive the azimuthal elastic impedance (AEI) using the derived reflection coefficient as

$$\mathrm{AEI}(\theta,\phi) = M^{a_M(\theta)}\,\mu^{a_\mu(\theta)}\,\rho^{a_\rho(\theta)}\,\exp\left[2a_{\rm N}(\theta,\phi)\delta_{\rm N} + 2a_{\rm T}(\theta,\phi)\delta_{\rm T}\right]. \tag{3}$$

Based on the derived AEI, we formulate the convolutional model for the case of n reflection interface as

$$\mathbf{d} = \mathbf{G}\mathbf{m} = \mathbf{W}\,\mathbf{D}\,\mathbf{m}, \tag{4}$$

where

$$\mathbf{d} = \begin{bmatrix} s_1(\theta,\phi) \\ s_2(\theta,\phi) \\ \vdots \\ s_n(\theta,\phi) \end{bmatrix}_{n\times 1}, \quad \mathbf{W} = \begin{bmatrix} w_1 & 0 & \dots & \dots & 0 \\ w_2 & w_1 & \ddots & \vdots & \vdots \\ \vdots & w_2 & \ddots & 0 & \vdots \\ \vdots & \vdots & \ddots & w_1 & 0 \\ w_n & w_{n-1} & \dots & w_2 & w_1 \end{bmatrix}_{n\times n},$$

$$\mathbf{D} = \begin{bmatrix} -1/2 & 1/2 & & & \\ & -1/2 & 1/2 & & \\ & & \ddots & \ddots & \\ & & & -1/2 & 1/2 \end{bmatrix}_{n\times(n+1)}, \quad \mathbf{m} = \begin{bmatrix} \mathrm{LAEI}_1(\theta,\phi) \\ \mathrm{LAEI}_2(\theta,\phi) \\ \vdots \\ \mathrm{LAEI}_{n+1}(\theta,\phi) \end{bmatrix}_{(n+1)\times 1}, \tag{5}$$

where $s_1, \ldots, s_n$, $w_1, \ldots, w_n$, and $\mathrm{LAEI}_1, \ldots, \mathrm{LAEI}_{n+1}$ represent samples of seismic data, wavelet, and logarithmic AEI, respectively.

Chen et al. (2015) propose a fractured anisotropic rock physics effective model. In the present study, we apply the fractured anisotropic rock physics model to well-logging data, and obtain curves of fracture weaknesses, as shown in Figure 1.

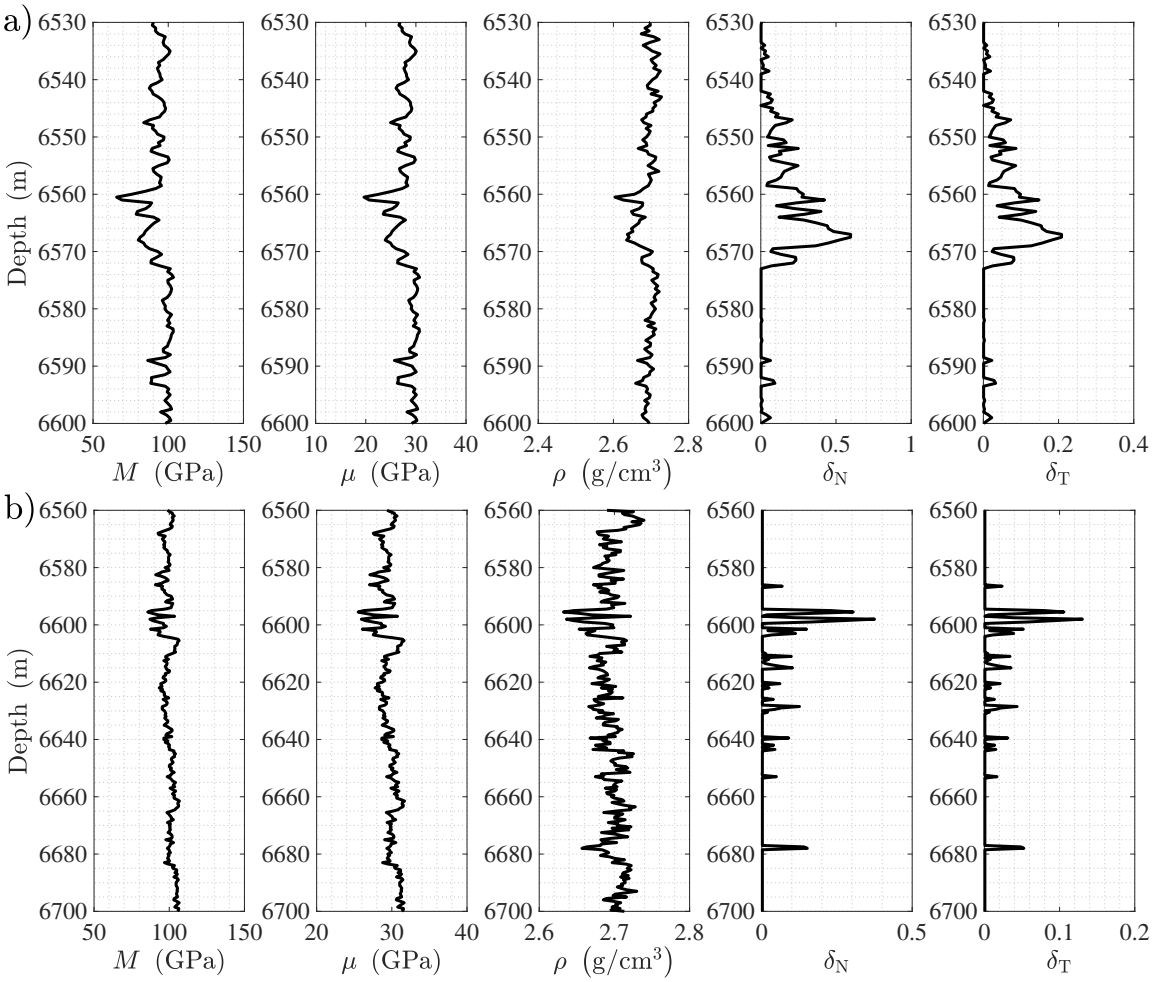

FIG. 1. Curves of P- and S-wave moduli, density and fracture weaknesses. a) well log 1; and b) well log 2.

Using the derived azimuthal elastic impedance, we calculate the AEI of incidence angles 6°, 16° and 26° and azimuthal angles 100° and 170°, and show the histograms of AEI in Figure 2. We observe a bimodal behavior of AEI, which can be approximately expressed using Gaussian mixture distributions.

Following Grana et al. (2017), we express the prior probability distribution function (PDF) $P(\mathbf{m})$ as a linear combination of Gaussian distributions

$$P(\mathbf{m}) = \sum_{k=1}^{2} \alpha_k \frac{1}{\sqrt{2\pi}\sigma_k} \exp\left[-\frac{1}{2}\frac{(\mathbf{m}-\bar{\mathbf{m}}_k)^T(\mathbf{m}-\bar{\mathbf{m}}_k)}{\sigma_k^2}\right], \tag{6}$$

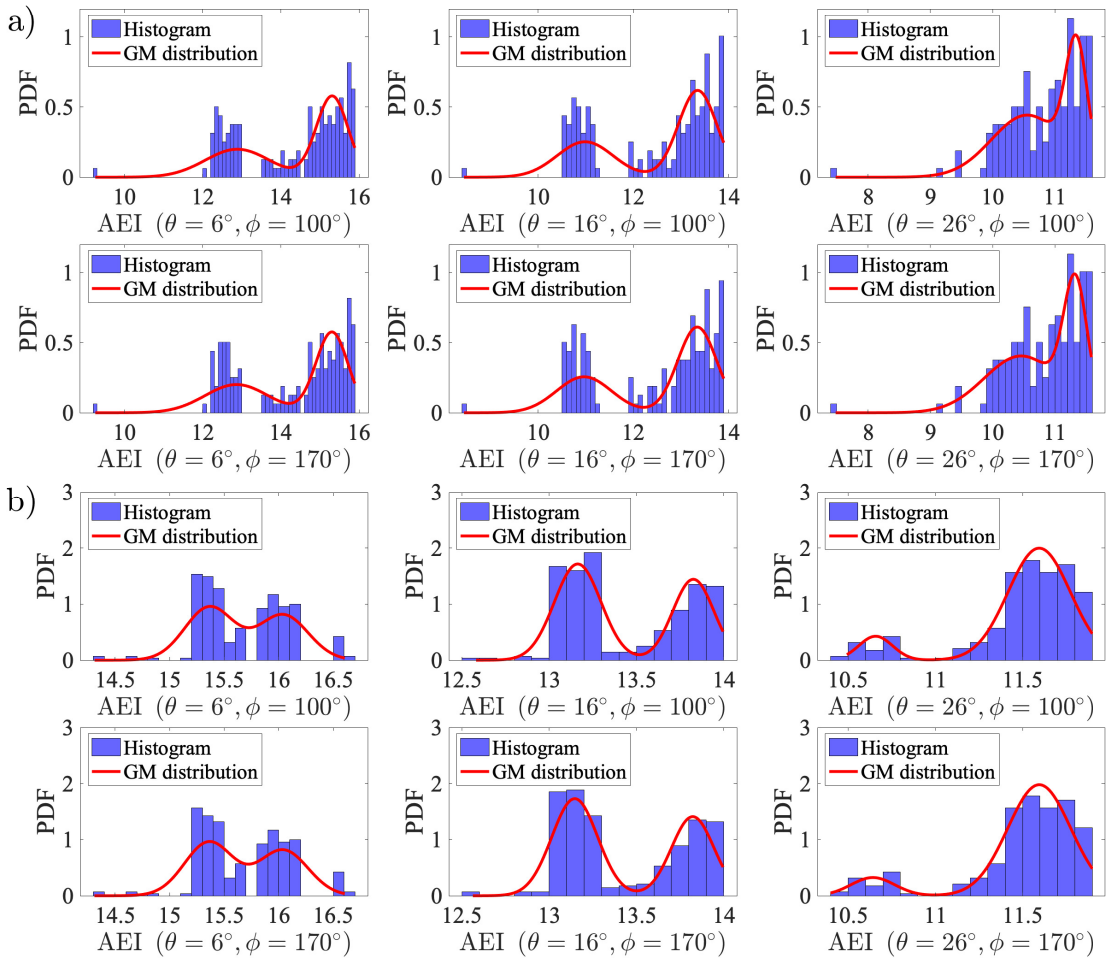

FIG. 2. Histograms of AEI. The solid red curves represent the smoothed gross histograms. a) well log 1; and b) well log 2.

where the coefficient α_k represents the weight of the linear combination, $\bar{\mathbf{m}}_k$ and σ_k^2 represent the mean and variance values of $\mathbf{m}$ of different fracture facies, respectively.

Under the assumption that seismic data contains Gaussian random noise, we express the likelihood function as

$$P(\mathbf{d}|\mathbf{m}) = \frac{1}{\sqrt{2\pi\sigma_{\mathbf{n}}^2}} \exp\left[-\frac{1}{2}\frac{(\mathbf{d}-\mathbf{G}\mathbf{m})^T(\mathbf{d}-\mathbf{G}\mathbf{m})}{\sigma_{\mathbf{n}}^2}\right], \tag{7}$$

where $\sigma_{\mathbf{n}}^2$ represents the variance of Gaussian random noise.

Combining equations 6 and 7, we express the posterior PDF as

$$\begin{aligned} P(\mathbf{m}|\mathbf{d}) = & \frac{1}{\sqrt{2\pi\sigma_{\mathbf{n}}^2}} \exp\left[-\frac{1}{2}\frac{(\mathbf{d}-\mathbf{G}\mathbf{m})^T(\mathbf{d}-\mathbf{G}\mathbf{m})}{\sigma_{\mathbf{n}}^2}\right] \\ & \times \left\{\sum_{k=1}^{2} \alpha_k \frac{1}{\sqrt{2\pi}\sigma_k} \exp\left[-\frac{1}{2}\frac{(\mathbf{m}-\bar{\mathbf{m}}_k)^T(\mathbf{m}-\bar{\mathbf{m}}_k)}{\sigma_k^2}\right]\right\}. \end{aligned} \tag{8}$$

Using the Bayesian Markov chain Monte Carlo (MCMC) method, we implement the inversion of azimuthal partially incidence-angle-stacked seismic data for estimating AEI of different incidence and azimuthal angles.

With the estimated AEI in hand, we proceed to the prediction of fracture facies. Using the seismic data and estimated AEI as the input, we express the posterior PDF, $P(\mathbf{f}|\mathbf{d},\mathbf{m})$, which is used to assess the fracture facies, as

$$P(\mathbf{f}|\mathbf{d},\mathbf{m}) \propto P(\mathbf{d}|\mathbf{m},\mathbf{f})\, P(\mathbf{m}|\mathbf{f})\, P(\mathbf{f}), \tag{9}$$

where $P(\mathbf{d}|\mathbf{m},\mathbf{f})$ is the distribution of seismic data given fracture facies and AEI, $P(\mathbf{m}|\mathbf{f})$ is the distribution of AEI in each fracture facies, and $P(\mathbf{f})$ is the distribution of fracture facies, respectively.

Based on the expressed posterior PDF, we employ the naive Bayesian classification method to obtain the fracture facies at different incidence and azimuthal angles. However, the real subsurface fractured area should only correspond to one fracture facies, which is independent of incidence and azimuthal angles.

To obtain the unique and final fracture facies from all the estimated results at different incidence and azimuthal angles, we present a simple procedure that among the predicted fracture facies results, the one with the highest number of occurrences at all given incidence angles and azimuths is considered the most likely unique and final result.

Inversion of AEI for fracture weaknesses constrained by models constructed using facies

With the estimated AEI and fracture facies in hand, we proceed to the inversion of AEI for fracture weaknesses, in which we employ the models constructed using the estimated fracture facies to constrain the inversion.

Based on the derived AEI, we express the logarithmic AEI (LAEI) as

$$\mathrm{LAEI}(\theta,\phi) = a_M(\theta) L_M + a_\mu(\theta) L_\mu + a_\rho(\theta) L_\rho + 2a_{\mathrm{N}}(\theta,\phi)\delta_{\mathrm{N}} + 2a_{\mathrm{T}}(\theta,\phi)\delta_{\mathrm{T}}, \tag{10}$$

where L_M, L_μ and L_ρ represent logarithmic P- and S-wave moduli and density. In the case of one interface, three incidence angles and two azimuths, we write the LAEI succinctly as

$$\mathbf{y} = \mathbf{A}\mathbf{x}, \tag{11}$$

where

$$\mathbf{y} = \begin{bmatrix} \mathrm{LAEI}(\theta_1,\phi_1) \\ \mathrm{LAEI}(\theta_2,\phi_1) \\ \mathrm{LAEI}(\theta_3,\phi_1) \\ \mathrm{LAEI}(\theta_1,\phi_2) \\ \mathrm{LAEI}(\theta_2,\phi_2) \\ \mathrm{LAEI}(\theta_3,\phi_2) \end{bmatrix}, \quad \mathbf{x} = \begin{bmatrix} L_M \\ L_\mu \\ L_\rho \\ \delta_{\mathrm{N}} \\ \delta_{\mathrm{T}} \end{bmatrix},$$

$$\mathbf{A}=\begin{bmatrix} a_M(\theta_1) & a_\mu(\theta_1) & a_\rho(\theta_1) & a_{\mathrm{N}}(\theta_1,\phi_1) & a_{\mathrm{T}}(\theta_1,\phi_1) \\ a_M(\theta_2) & a_\mu(\theta_2) & a_\rho(\theta_2) & a_{\mathrm{N}}(\theta_2,\phi_1) & a_{\mathrm{T}}(\theta_2,\phi_1) \\ a_M(\theta_3) & a_\mu(\theta_3) & a_\rho(\theta_3) & a_{\mathrm{N}}(\theta_3,\phi_1) & a_{\mathrm{T}}(\theta_3,\phi_1) \\ a_M(\theta_1) & a_\mu(\theta_1) & a_\rho(\theta_1) & a_{\mathrm{N}}(\theta_1,\phi_2) & a_{\mathrm{T}}(\theta_1,\phi_2) \\ a_M(\theta_2) & a_\mu(\theta_2) & a_\rho(\theta_2) & a_{\mathrm{N}}(\theta_2,\phi_2) & a_{\mathrm{T}}(\theta_2,\phi_2) \\ a_M(\theta_3) & a_\mu(\theta_3) & a_\rho(\theta_3) & a_{\mathrm{N}}(\theta_3,\phi_2) & a_{\mathrm{T}}(\theta_3,\phi_2) \end{bmatrix}. \tag{12}$$

Under assumptions that the difference between the modeling LAEI data and the input LAEI result is Gaussian and the prior distribution of elastic properties (i.e. P- and S-wave moduli), density and fracture weaknesses is Cauchy, we express the posterior PDF $P(\mathbf{X}|\mathbf{Y})$ as

$$P(\mathbf{x}|\mathbf{y}) \propto P_0 \exp\left(-\frac{(\mathbf{y}-\mathbf{A}\mathbf{x})^T(\mathbf{y}-\mathbf{A}\mathbf{x})}{2\sigma_{\mathbf{d}}^2}\right)\exp\left[-\sum_{i=1}^{5}\ln\left(1+\frac{{x_i}^2}{\sigma_{\mathbf{x}}^2}\right)\right], \tag{13}$$

where $\sigma_{\mathbf{d}}^2$ is the variance of difference between the modeling and input AEI datasets, x_i is the element in the unknown parameter vector $\mathbf{x}$, $\sigma_{\mathbf{x}}^2$ is the variance of the unknown parameter vector, and P_0 is a constant that is related to $\sigma_{\mathbf{d}}^2$ and $\sigma_{\mathbf{x}}^2$, respectively.

Traditionally, inversion results and lithofacies prediction results are combined for reservoir and fluid prediction (Grana and Della Rossa, 2010; Grana et al., 2017, 2021). In the present study, we further utilize the predicted final fracture facies to build an initial model to constrain the inversion for the unknown parameter vector $\mathbf{x}$.

To build initial models of P- and S-wave moduli and density, we may employ the pre-stacked seismic data along the fracture strike azimuth to estimate P- and S-wave moduli and density roughly. Following Chen et al. (2020), we may roughly estimate the normal and tangential fracture weaknesses based on the extraction of AVO intercept and gradient.

With the roughly estimated P- and S-wave moduli, density and fracture weaknesses in hand, we further implement the low-frequency model building driven by the estimated fracture facies. Using the fractured facies obtained in the previous step, we build new models of L_M^{mod}, L_μ^{mod}, L_ρ^{mod}, $\delta_{\mathrm{N}}^{\mathrm{mod}}$ and $\delta_{\mathrm{T}}^{\mathrm{mod}}$ as

$$\begin{aligned} L_M^{\mathrm{mod}} &= L_M^{\mathrm{rough}} + s_M \times f, \\ L_\mu^{\mathrm{mod}} &= L_\mu^{\mathrm{rough}} + s_\mu \times f, \\ L_\rho^{\mathrm{mod}} &= L_\rho^{\mathrm{rough}} + s_\rho \times f, \\ \delta_{\mathrm{N}}^{\mathrm{mod}} &= \delta_{\mathrm{N}}^{\mathrm{rough}} + s_{\mathrm{N}} \times f, \\ \delta_{\mathrm{T}}^{\mathrm{mod}} &= \delta_{\mathrm{T}}^{\mathrm{rough}} + s_{\mathrm{T}} \times f, \end{aligned} \tag{14}$$

where L_M^{rough}, L_μ^{rough}, L_ρ^{rough}, $\delta_{\mathrm{N}}^{\mathrm{rough}}$ and $\delta_{\mathrm{T}}^{\mathrm{rough}}$ represent the roughly estimated P- and S-wave moduli and density and fracture weaknesses, s_M, s_μ, s_ρ, s_{N} and s_{T} represent scale factors that determine how fracture facies contributes to the constructed models, and f represents the estimated fracture facies.

Low-frequency components of new models are used as initial models to constrain the inversion. The objective function, which is proposed to obtain maximum a posterior (MAP)

solution and constrained by initial models, is given by

$$J(\mathbf{x}) = \frac{(\mathbf{y}-\mathbf{A}\mathbf{x})^T(\mathbf{y}-\mathbf{A}\mathbf{x})}{2\sigma_{\mathbf{d}}^2} + \sum_{i=1}^{5}\ln\left(1+\frac{{x_i}^2}{\sigma_{\mathbf{x}}^2}\right) + (\mathbf{x}-\mathbf{x}_{\mathrm{mod}})^T(\mathbf{x}-\mathbf{x}_{\mathrm{mod}}), \quad (15)$$

where $\mathbf{x}_{\mathrm{mod}}$ represents the vector of model constraints involving L_μ^{mod}, L_ρ^{mod}, $\delta_{\mathrm{N}}^{\mathrm{mod}}$ and $\delta_{\mathrm{T}}^{\mathrm{mod}}$.

Solving $\partial J(\mathbf{x})/\partial\mathbf{x} = 0$, we obtain the inversion results of $\mathbf{x}$. The Iterative re-weighed least squares (IRLS) method proposed by Alemie (2010) is employed to obtain the final inversion results of P- and S-wave moduli, density and fracture weaknesses.

RESULTS

In this section, noisy synthetic data are generated to verify the robustness of the proposed inversion method. We further apply the inversion method to real data to estimate elastic properties and fracture weaknesses.

Synthetic examples

Using a well log model, we first generate synthetic data of different incidence and azimuthal angles. In Figure 3, we show curves of P- and S-wave moduli, density and fracture weaknesses of the well log model.

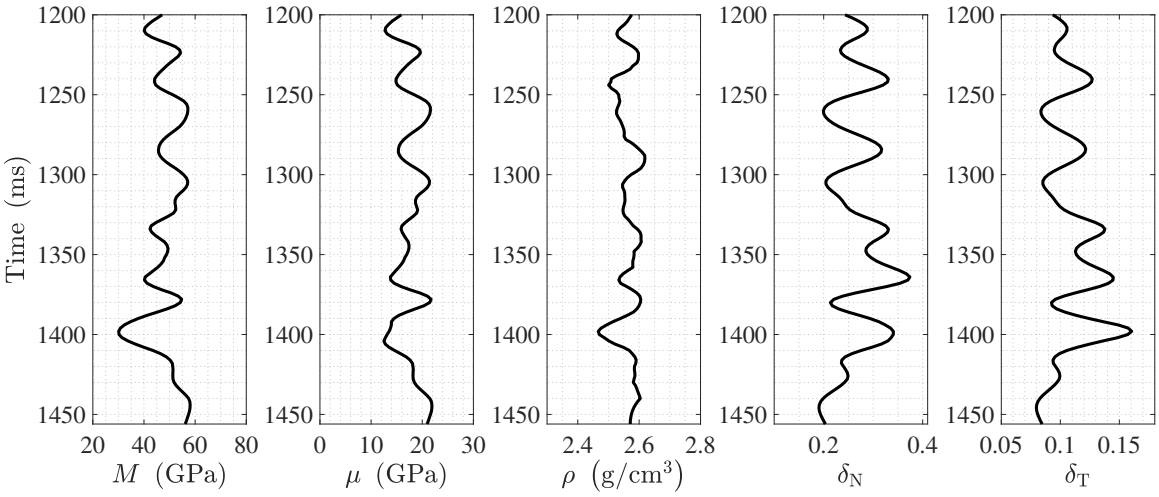

FIG. 3. Curves of P- and S-wave moduli, density and fracture weaknesses of well log model.

Using the formulated convolutional model shown in equation 4, we generate synthetic seismic gathers of incidence angles $1^\circ - 30^\circ$ and azimuths $\phi_1 = 5^\circ$ and $\phi_2 = 85^\circ$, and add Gaussian random noise to the synthetic seismic gathers to obtain noisy seismic gathers of signal-to-noise ratio (S/N) of 4 and 1, as shown in Figure 4.

Using the proposed inversion method, we implement the inversion of partially incidence-angle-stacked seismic gathers for estimating AEI of $\theta_1 = 5^\circ$, $\theta_2 = 15^\circ$ and $\theta_3 = 25^\circ$ at

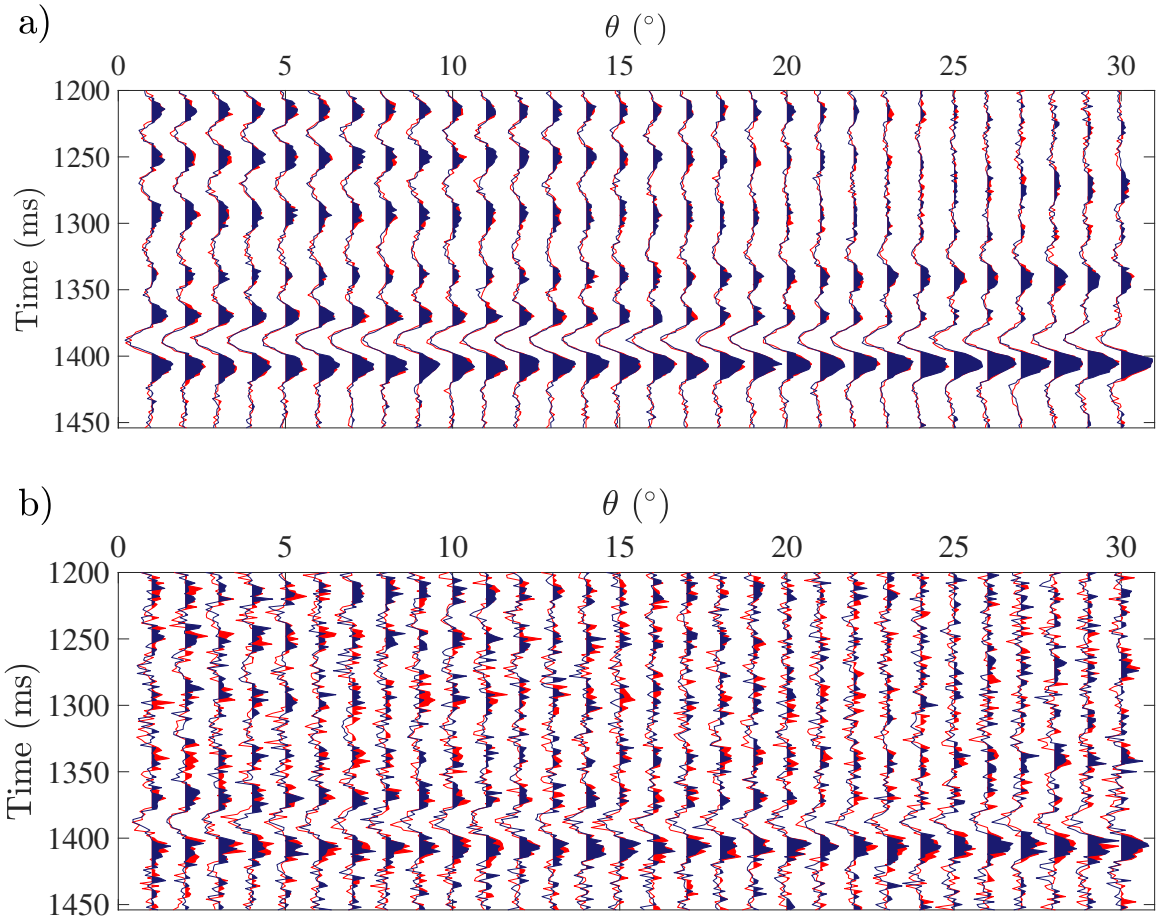

FIG. 4. Noisy seismic data. a) S/N of 4, and (b) S/N of 1. Seismic gathers of azimuths $\phi_1 = 5°$ and $\phi_2 = 85°$ are plotted in red and blue, respectively.

azimuths ϕ_1 and ϕ_2. Using the estimate AEI and seismic data as the input, we implement the prediction of fracture facies at each incidence and azimuthal angles. Comparisons between true values calculated using the presented AEI equation and the corresponding inversion results and the predicted fracture facies are shown in Figures 5 and 6.

Using the estimated fracture facies at different incidence and azimuthal angles, we further obtain the final fracture facies results based on the procedure of selecting the facies with the highest number of occurrences as the most likely unique and final result. In Figure 7, we show the obtained final fracture facies for the case of S/N of 4 and 1. We attach the curve of AEI (θ_1, ϕ_1) next to the predicted fracture facies, and observe that in the area where the AEI shows a significantly low value (around 1400 ms), the fracture facies appears.

We further implement the inversion of AEI for estimating elastic parameters and fracture weaknesses. Comparisons between true values, new models constructed using the estimated fracture facies and traditional low-frequency models are shown in Figure 8.

Using two different models, we implement the inversion for M, μ, ρ, δ_{N} and δ_{T}. Comparisons between true values, inversion results obtained using the new model constraint

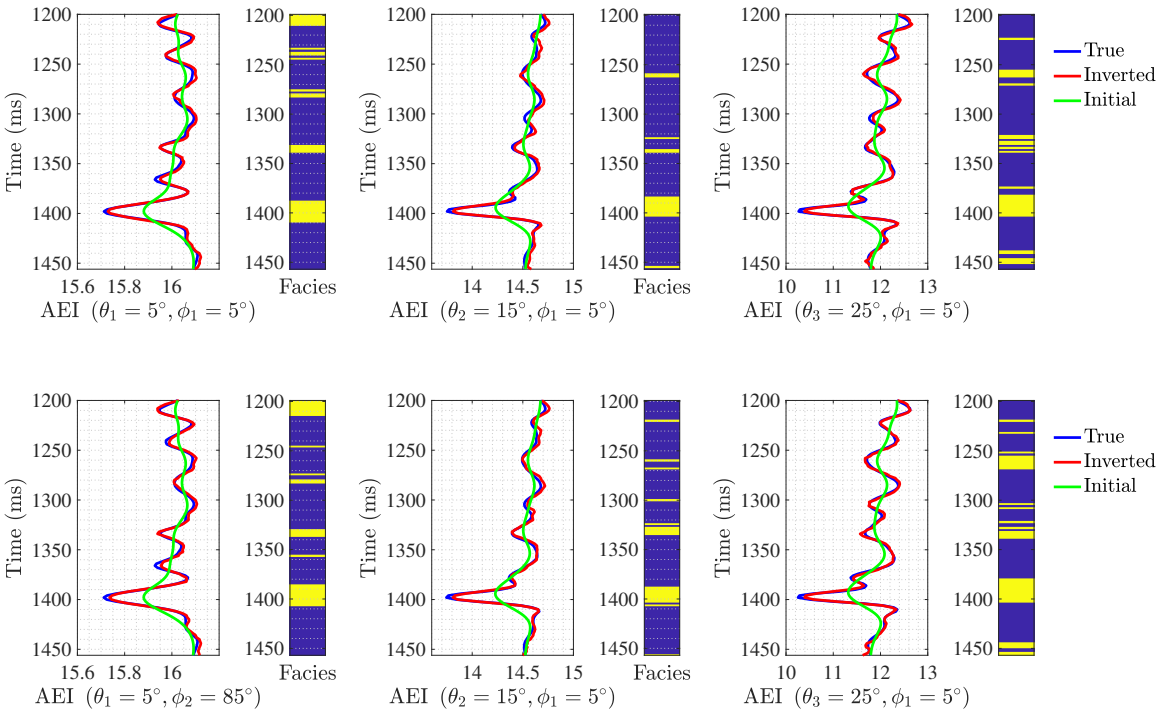

FIG. 5. Comparisons between true values and inversion results of AEI and the predicted fracies at incidence angles θ_1, θ_2, θ_3 and azimuths ϕ_1 and ϕ_2 in the case of S/N of 4. Initial model is a smoothed version of the true value. Fractured layers are in yellow, and non-fractured layers are in blue.

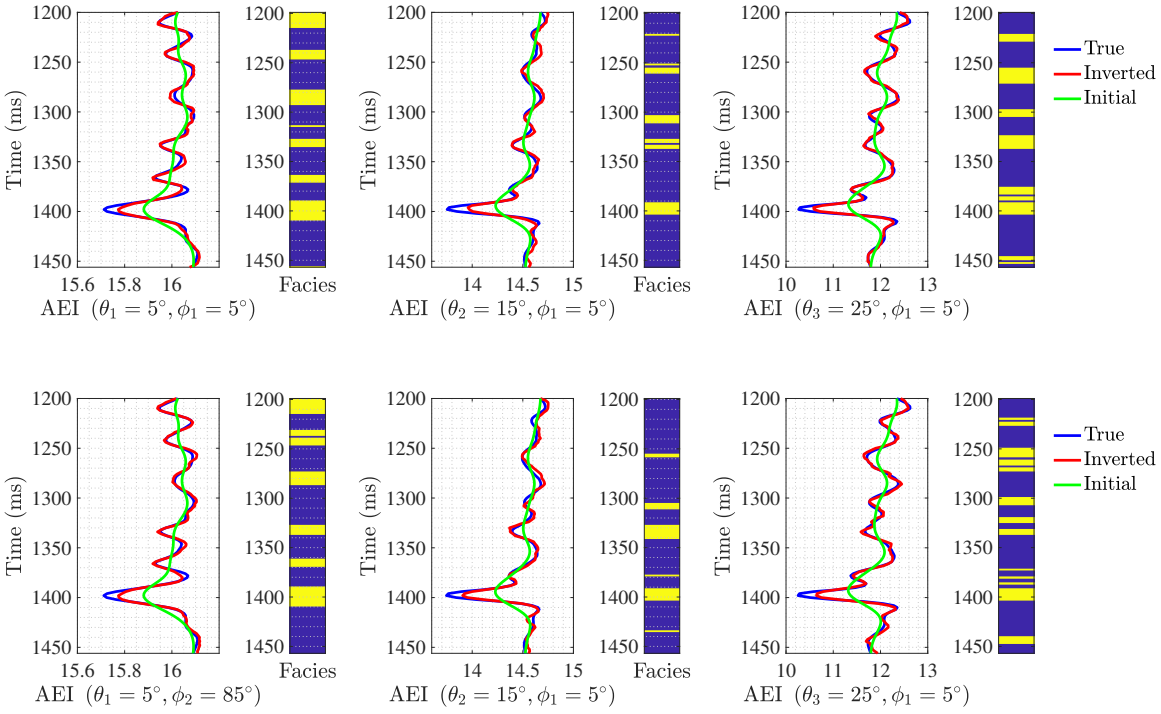

FIG. 6. Comparisons between true values and inversion results of AEI and the predicted fracies at incidence angles θ_1, θ_2, θ_3 and azimuths ϕ_1 and ϕ_2 in the case of S/N of 1. Initial model is a smoothed version of the true value. Fractured layers are in yellow, and non-fractured layers are in blue.

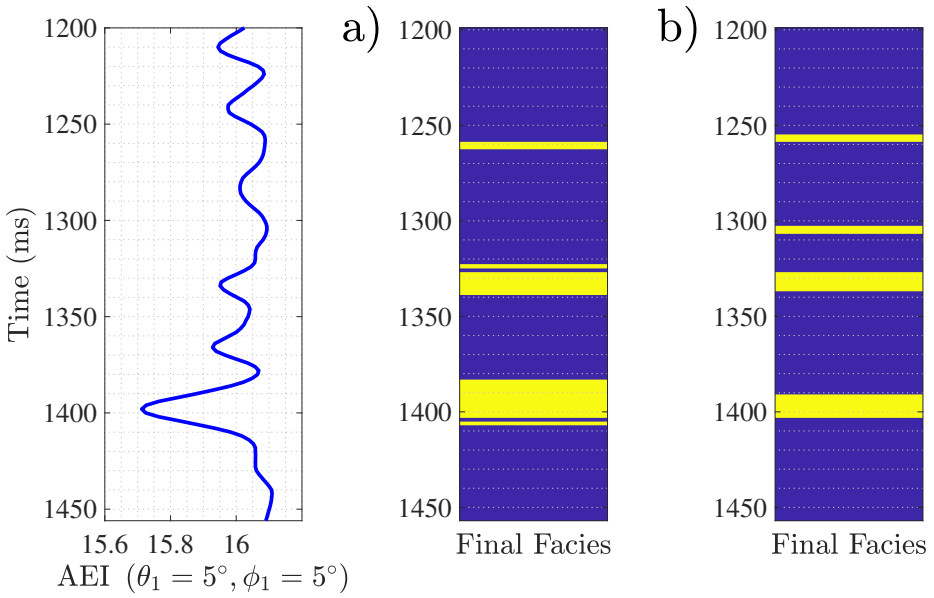

FIG. 7. Final fracture facies. a) S/N of 4; and b) S/N of 1. Fractured layers are in yellow, and non-fractured layers are in blue.

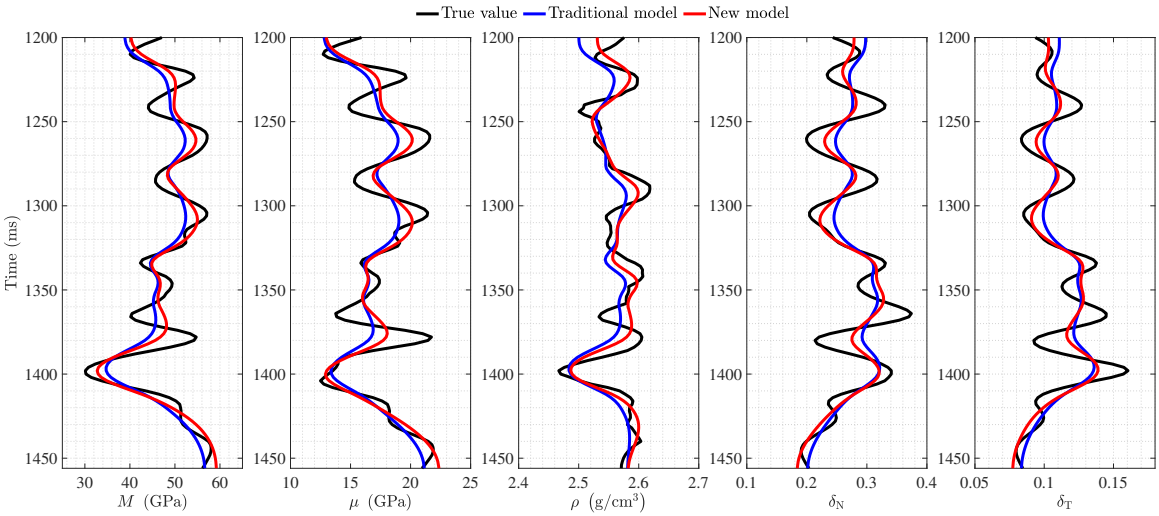

FIG. 8. Comparisons between true values (black), new constructed models (red) and traditional models (blue).

and that obtained using the traditional model constraint are shown in Figure 9.

We observe that the results obtained using the proposed inversion method constrained by the new constructed models match the true value better than that obtained using the inversion method constrained by the traditional low-frequency models. Even in the case of employing noisy seismic data of S/N of 1 as the input, we may obtain good inversion results of elastic parameters and fracture weaknesses, which verifies the robustness of the proposed inversion method.

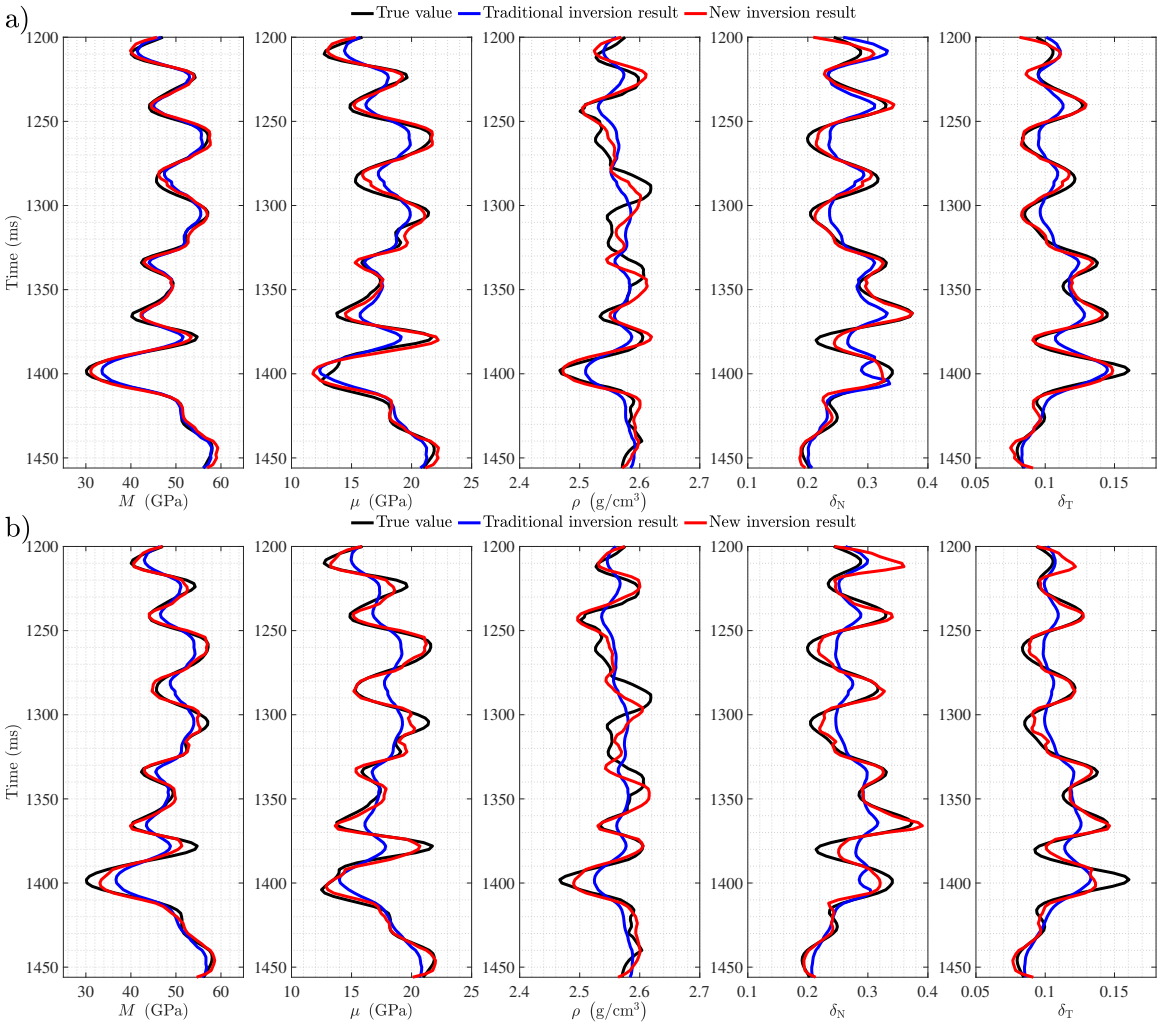

FIG. 9. Comparisons between true values (black), inversion results obtained using new model constraints (red) and that obtained using traditional model constraints (blue) of elastic parameters and fracture weaknesses. a) S/N of 4; and b) S/N of 1.

Real data example

We proceed to applying the proposed inversion method to observed seismic data to clarify how to obtain reliable results of fracture weaknesses in the real world case.

In Figure 10, we plot the partially incidence-angle-stacked seismic data at two azimuths. Using the proposed inversion method, we first implement the estimation of AEI considering a Gaussian mixture prior distribution, and predict the fracture facies at the given incidence angle and azimuths, as shown in Figures 11 and 12. We observe in the location where P-wave velocity provided by well log shows relatively low values, the estimated AEI also exhibits relative low values and fracture facies appears.

Again we implement the selection of unique and final fracture facies using the estimated results at these incidence and azimuthal angles. In Figure 13, we show the final fracture facies, which is employed to build the new model constraints for the sequential inversion. In Figure 14, we show the new models of P- and S-wave moduli, density and fracture weak-

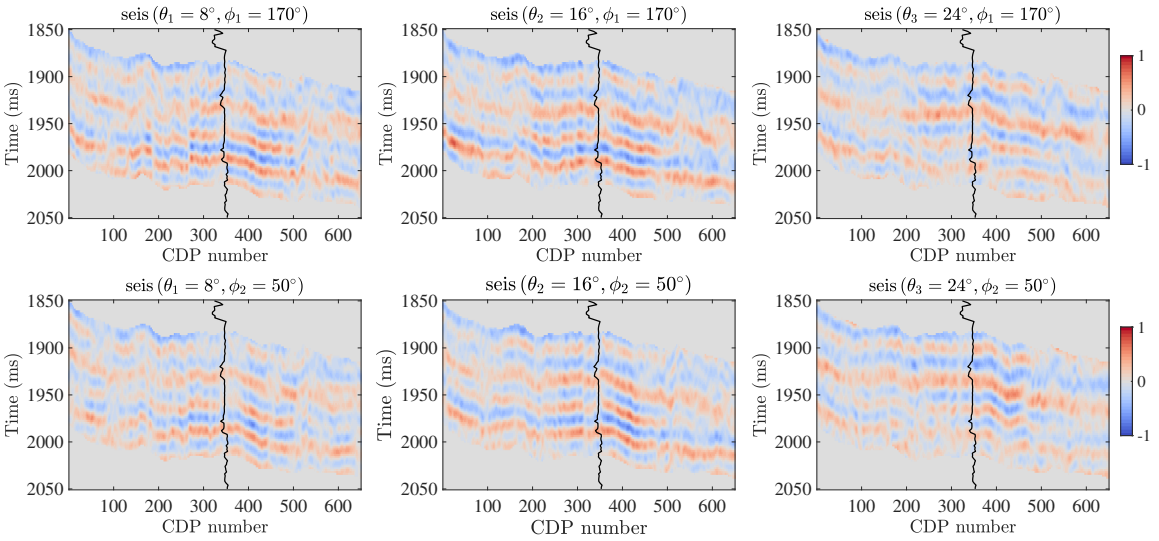

FIG. 10. Partially incidence-angle-stacked seismic data. The curve represents P-wave velocity provided by well logging data

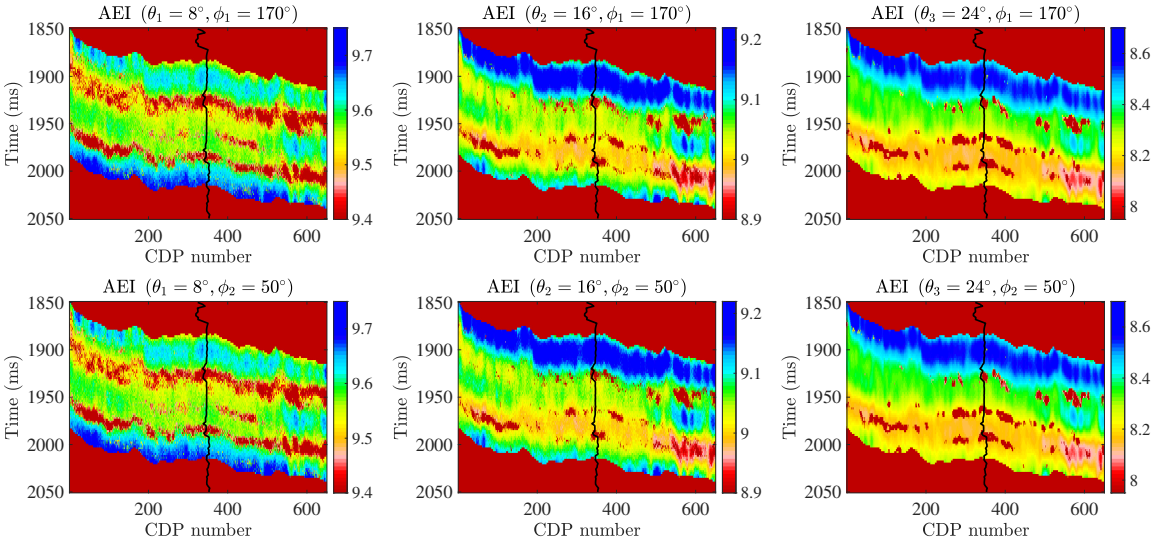

FIG. 11. Inversion results of AEI of three incidence angles and two azimuths. The curve represents P-wave velocity provided by well logging data.

nesses. Using new constructed models, we implement the inversion for elastic parameters and fracture weaknesses, as shown in Figure 15.

We observe in the location where P- and S-wave moduli and density exhibit relatively low values, the estimated fracture weaknesses show relatively high values, and these layers correspond to the intervals with low values of P-wave velocity curve. It reveals that using the proposed inversion method we may obtain reliable results of elastic parameters and fracture weaknesses.

CONCLUSION

To improve accuracy of estimating fracture weaknesses of underground layers, we propose a two-stage inversion method, which is implemented as: 1) employing azimuthal

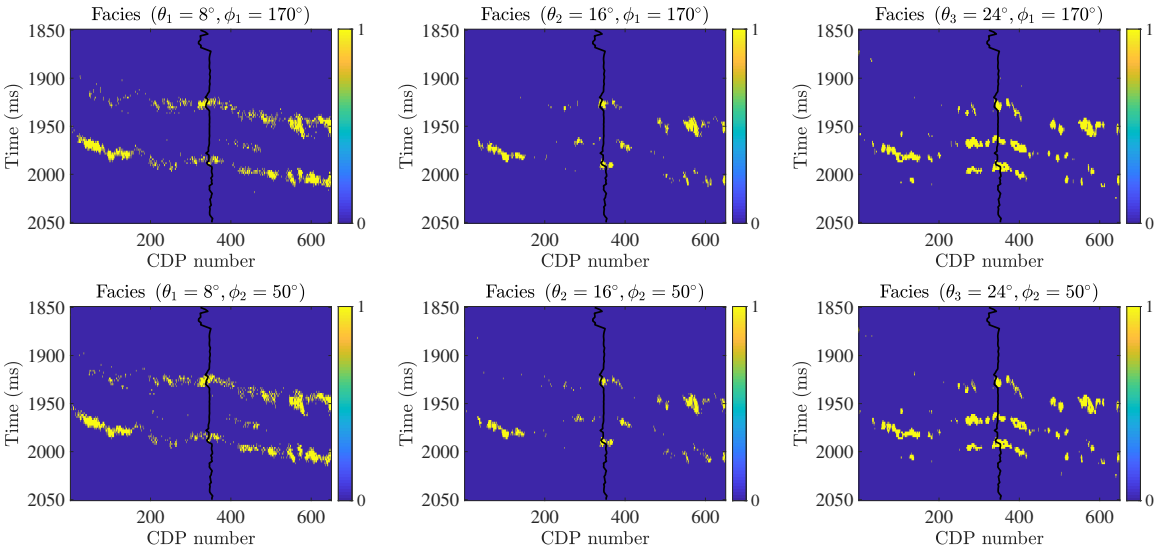

FIG. 12. Predicted fracture facies at three incidence angles and two azimuths. The curve represents P-wave velocity provided by well logging data. Fractured layers are in yellow, and non-fractured layers are in blue.

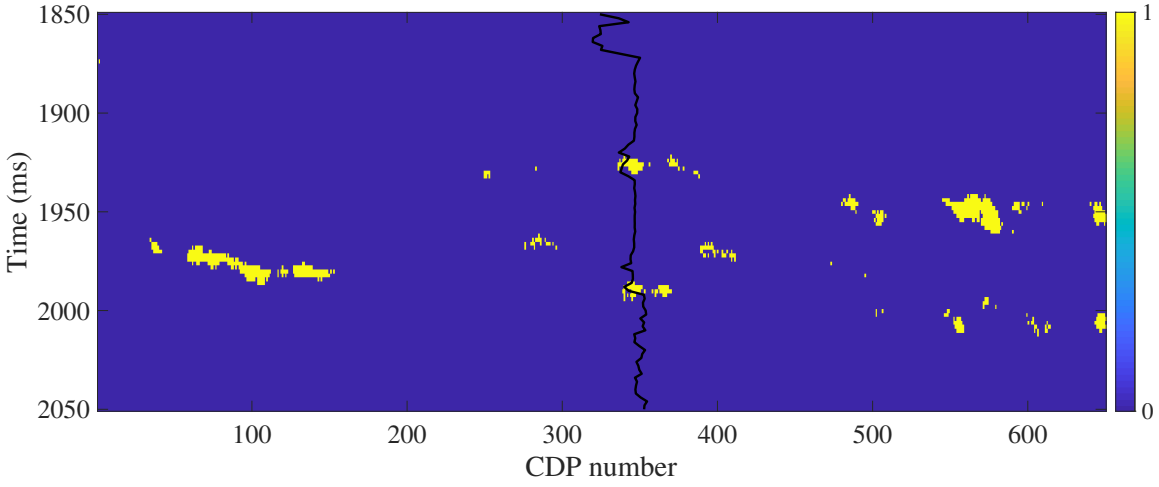

FIG. 13. Final fracture facies selected using all the estimated results at three incidence angles and two azimuths. The curve represents P-wave velocity provided by well logging data. Fractured layers are in yellow, and non-fractured layers are in blue.

seismic data to estimate AEI and predict fracture facies, and 2) using the estimated AEI to obtain elastic parameters and fracture weaknesses constrained by new models constructed using the predicted fracture facies.

In the first stage, we assume Gaussian mixture prior distribution and implement the Bayesian MCMC inversion for AEI of different incidence and azimuthal angles and predict fracture facies according to Bayesian classification. In the second stage, we use the predicted fracture facies to build new initial models for the sequential maximum a posterior (MAP) inversion for elastic parameters and fracture weaknesses.

Synthetic noisy seismic data are used to verify the robustness of the proposed inversion method. Comparisons between inversion results and true values of P- and S-wave moduli,

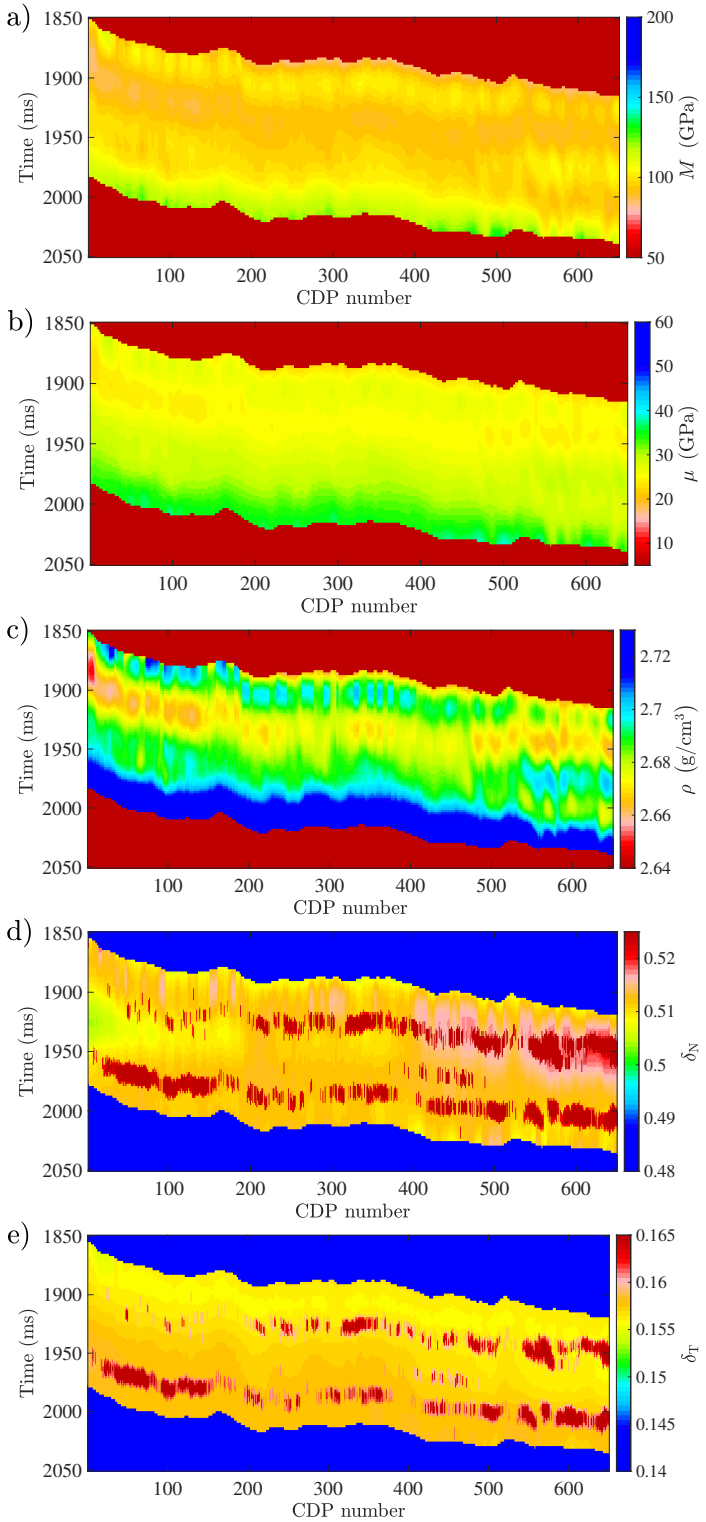

FIG. 14. New models constructed based on the fracture facies. a) P-wave modulus M, b) S-wave modulus μ, c) Density ρ, d) The normal fracture weakness δ_N and e) The tangential fracture weakness δ_T.

density and fracture weaknesses reveal that the inversion constrained by new models constructed based on the predicted fracture facies can produce elastic parameters and fracture

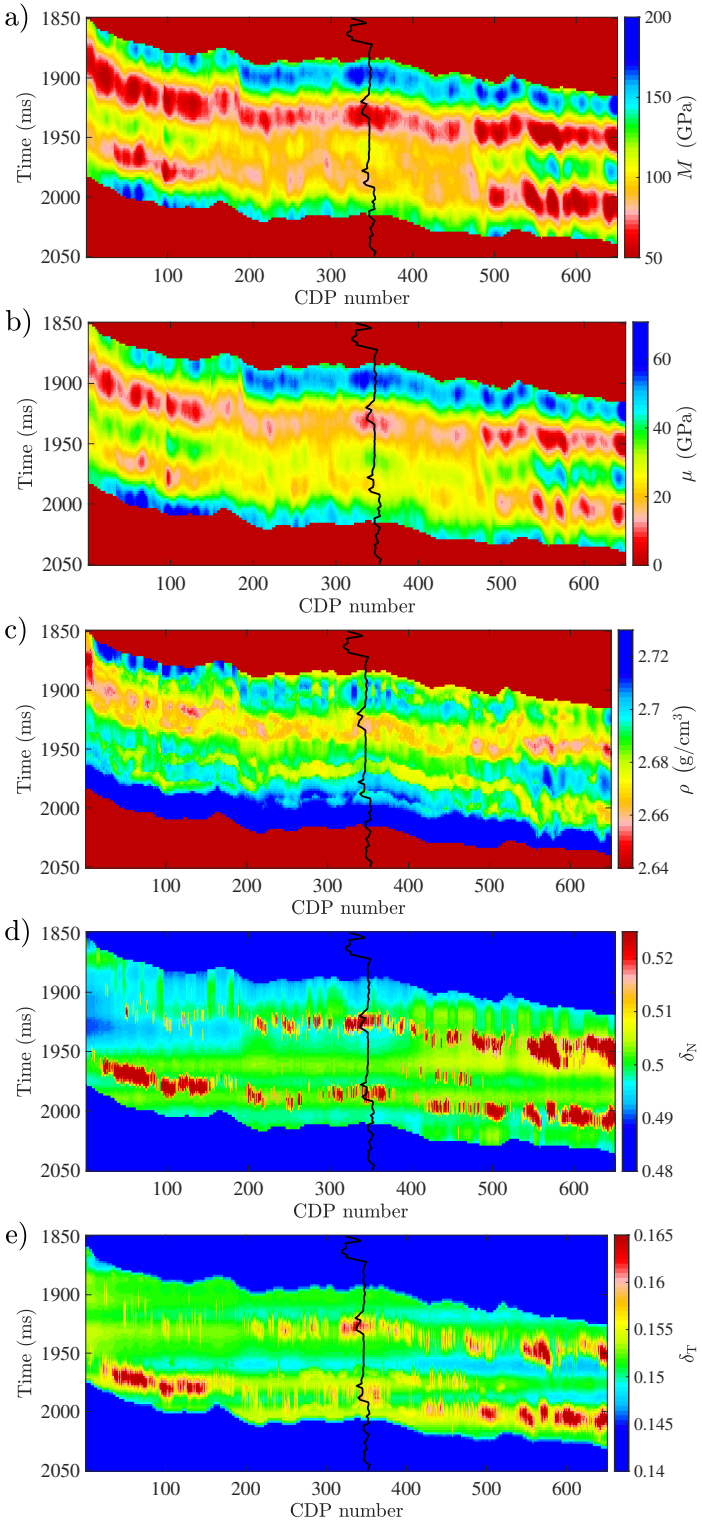

FIG. 15. Inversion results obtained using new model constraints. a) P-wave modulus M, b) S-wave modulus μ, c) Density ρ, d) The normal fracture weakness δ_N and e) The tangential fracture weakness δ_T. The curve represents P-wave velocity provided by well log.

weaknesses that better match the true values than the inversion constrained by traditional low frequency modes. Real data example shows that the proposed two-stage inversion

method can be used to generate reliable fracture weaknesses that act as additional indicators for the characterization of underground fractured layers.

ACKNOWLEDGMENTS

This study was funded by the National Natural Science Foundation of China (42104109, 42274162) and also supported by the Natural Science Foundation of Shanghai (21ZR1464700).

REFERENCES

Alemie, W. M., 2010, Regularization of the AVO inverse problem by means of a multivariate Cauchy probability distribution: M.Sc. thesis, University of Alberta.

Chen, H., Chen, T., and Innanen, K. A., 2020, Estimating tilted fracture weaknesses from azimuthal differences in seismic amplitude data: Geophysics, **85**, No. 3, R135–R146.

Chen, H., Ji, Y., and Innanen, K. A., 2018, Estimation of modified fluid factor and dry fracture weaknesses using azimuthal elastic impedance: Geophysics, **83**, No. 1, WA73–WA88.

Chen, H., Yin, X., Gao, J., Liu, B., and Zhang, G., 2015, Seismic inversion for underground fractures detection based on effective anisotropy and fluid substitution: Science China Earth Sciences, **58**, 805–814.

Chen, H., Zhang, G., Ji, Y., and Yin, X., 2017, Azimuthal seismic amplitude difference inversion for fracture weakness: Pure and Applied Geophysics, **174**, No. 1, 279–291.

Grana, D., 2018, Joint facies and reservoir properties inversion: Geophysics, **83**, No. 3, M15–M24.

Grana, D., and Della Rossa, E., 2010, Probabilistic petrophysical-properties estimation integrating statistical rock physics with seismic inversion: Geophysics, **75**, No. 3, O21–O37.

Grana, D., Fjeldstad, T., and Omre, H., 2017, Bayesian Gaussian mixture linear inversion for geophysical inverse problems: Mathematical Geosciences, **49**, 493–515.

Grana, D., Mukerji, T., and Doyen, P., 2021, Seismic reservoir modeling: Theory, examples, and algorithms: John Wiley & Sons.

Hudson, J., 1980, Overall properties of a cracked solid: Mathematical Proceedings of the Cambridge Philosophical Society, **88**, 371–384.

Li, K., Yin, X., Zong, Z., and Grana, D., 2022, Estimation of porosity, fluid bulk modulus, and stiff-pore volume fraction using a multitrace Bayesian amplitude-variation-with-offset petrophysics inversion in multiporosity reservoirs: Geophysics, **87**, No. 1, M25–M41.

Schoenberg, M., and Douma, J., 1988, Elastic wave propagation in media with parallel fractures and aligned cracks1: Geophysical prospecting, **36**, No. 6, 571–590.